Journal of ELECTRONIC MATERIALS, Vol. 47, No. 2, 2018
https://doi.org/10.1007/s11664-017-5983-x

Magnetic Interaction at the Interface of Epitaxial Manganite Film and an Intermetallic Superlattice

A.S. GRISHIN,[1,2,5] G.A. OVSYANNIKOV,[1] A.A. KLIMOV,[1,2] V.V. DEMIDOV,[1] K.Y. CONSTANTINIAN,[1] I.V. BORISENKO,[1] V.L. PREOBRAZHENSKY,[3,4] N. TIERCELIN,[4] and P. PERNOD[4]

1.—Joint International Laboratory LIA LICS, Kotel'nikov Institute of Radio Engineering and Electronics, Russian Academy of Sciences, 11 Mokhovaya Str., Moscow, Russia 125009. 2.—Joint International Laboratory LIA LICS, Moscow Technological University MIREA, 86 Vernadsky Av., Moscow, Russia 119571. 3.—Joint International Laboratory LIA LICS, The Wave Research Center, Prokhorov General Physics Institute, Russian Academy of Sciences, 38 Vavilova Str., Moscow, Russia 119991. 4.—Joint International Laboratory LIA LICS, Univ. Lille, CNRS, Centrale Lille, ISEN, Univ. Valenciennes, UMR8520 – IEMN, 59000 Lille, France. 5.—e-mail: alex1995@hitech.cplire.ru

Hybrid magnetic heterostructures made of epitaxial manganite $La_{0.7}Sr_{0.3}MnO_3$ thin film and an intermetallic superlattice $(TeCo_2/FeCo)_n$ were prepared on orthorhombic $NdGaO_3$ substrates and characterized by means of magneto-optical Kerr effect, magnetoresistance and ferromagnetic resonance. Experimental data show that magnetic interaction between $La_{0.7}Sr_{0.3}MnO_3$ and $(TeCo_2/FeCo)_n$ is of an antiferromagnetic nature. The features observed in magnetotransport characteristics are caused by the magnetization reversal at the interface between manganite thin film and intermetallic superlattice.

Key words: Epitaxial thin films, manganites, intermetallic superlattice, interface, Kerr effect, ferromagnetic resonance, magnetoresistance

INTRODUCTION

The development of spintronic devices based on nanoscale interfaces of magnetic materials is a challenging problem.[1] Stacks of complex materials (manganites, multiferroics, rare earth compounds and others) for non-volatile memory devices were reviewed in Refs. 2 and 3. Manipulation of phase transition in manganite $La_{0.7}Sr_{0.3}MnO_3$(LSMO) thin film was achieved by applying positive/negative voltage over an additional gate electrode.[4] Large tunneling resistance effect, accompanied with a moderately magnetoresistance was reported for LSMO/$BaTiO_3$/Co junctions.[5] Recently, a promising solution was proposed for memory cells providing reliable spin manipulation and switching of magnetization between two stable positions in intermetallic structures.[6,7] The solution is based on a superlattice of exchange-coupled rare-earth compound $TbCo_2$ and 3*d* transition metal FeCo nanolayers. The structure is characterized by a giant magnetostriction and demonstrates spin reorientation transitions by means of an external magnetic field, and/or elastic strain.[1,8–14] In transition metal oxides ($R_{1-x}A_xMnO_3$, manganites), where *R* is one of the rare earth elements La or Pr and A is one of the alkaline earth metals Sr or Ca, new electronic states and magnetic phases can arise under electric field and strain in thin film or at the interfaces with dielectrics or other oxides.[12,15] However, the magnetic interaction and electronic and spin states at the interface between manganites and intermetallic structures have not yet been studied in detail. In this paper, we fabricated manganite/intermetallic heterostructures in order to determine magnetization behavior at the interface and to reveal the influence of spin-polarized current on magnetotransport characteristics. The preliminary data for this paper was published previously in Ref. 12.

(Received April 28, 2017; accepted November 20, 2017; published online December 1, 2017)

Based on Ref. 12, we estimated the influence of the interlayer interaction at the interfaces of the manganite and the superlattice, and measured the magnetoresistance in order to determine its type and the specificity of the contribution of the interlayer interaction. We also studied high-frequency properties of the structure and determined the type of magnetic interaction between manganite and intermetallic layers using the ferromagnetic resonance data.

SAMPLE FABRICATION AND EXPERIMENTAL

The heterostructures under consideration consist of two layers. The top layer is the rare earth intermetallic superlattice, consisting of an exchange-coupled multilayered [$TbCo_2$ (4 nm)/FeCo(4 nm)]n (TCFC) stack with n = 25. The bottom layer is the lanthanum–strontium manganite $La_{0.7}Sr_{0.3}MnO_3$ (LSMO) 30-nm-thick film which was epitaxially deposited on an orthorhombic $NdGaO_3$ (NGO) substrate.

The LSMO films were deposited onto 5 × 5 × 0.5-mm^3(110) NGO substrates by magnetron sputtering at 750–800 °C with oxygen pressure between 0.1 and 0.3 mbar. The desired crystal structure of the LSMO film was ensured by the lattice parameters of NGO substrate that promoted the dominance of uniaxial in-plane magnetic anisotropy.[14,16] The intermetallic superlattice was obtained by the sequential sputtering of $TbCo_2$ and FeCo nanolayers under applied magnetic field directed in the plane of the substrate that defined the direction of the uniaxial easy axis magnetic anisotropy.[9,11,12] The strength of the magnetic anisotropy in the TCFC superlattice is controlled by the ratio of Tb, Co, and Fe elements in the layers as well as by the thickness and number n of $TbCo_2$ and FeCo layers. The heterostructures were fabricated with directions of easy axis magnetization of the manganite and intermetallic superlattice being in parallel. The LSMO film covers the whole 5 × 5-mm^2 area of the substrate, whereas the TCFC is a 3 × 3-mm^2 square at the center of the sample (Fig. 1).

Magnetic parameters, the coercive force (H_C) and saturation field (H_S), of heterostructure were studied using magneto-optical Kerr effect (MOKE). The magneto-optical setup comprises a semiconductor laser operating at a wavelength of λ = 0.63 μm and power P = 5 mW, a beam-splitter glass plate for forming the reference and signal beams, a $\lambda/2$ thick phase-shifter plate for selecting the s- or p-type polarization of the incident beam, and a polarizer/analyzer for selecting the signal caused by the meridional Kerr effect. The laser spot diameter at the measuring point is about 1 mm. The investigated sample was placed on a rotary table in the gap of an H-field electromagnet. The angle (δ) of polarization plane rotation of the beam reflected from the surface of the magnetized sample was determined

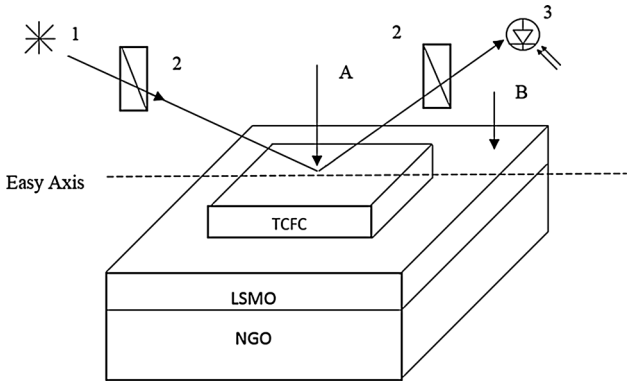

Fig. 1. Schematic view of the investigated heterostructures and MOKE geometry: He-Ne laser (1), polarizers (2), detector (3). "A" and "B" are respectively the spot positions where TCFC/LSMO structure and LSMO film only were probing.

by the compensation method using the polarizer-analyzer. The dependence $\delta(H)/\delta_S \propto M(H)/M_S$ was measured, where δ_S is the MOKE signal at $M = M_S$ (M_S is the saturation magnetization of the sample). A detailed description of the experimental setup is given in Ref. 6. The vibrating sample magnetometer (VSM), and the ferromagnetic resonance (FMR) spectrometer were used for heterostructure characterization as well. Magnetoresistance $R(H)$ dependencies were obtained by measuring the differential resistance $R = dV/dI$ as a function of the applied magnetic field H. The Curie temperatures (T_C) for both TCFC and LSMO films were well above room temperature (300 K) where most of the measurements were carried out. Nevertheless, some of the resistive characteristics for higher accuracy were measured at 77 K by the 4-point method.

RESULTS AND DISCUSSION

Kerr Effect Measurements

The magnetic field dependence of magnetization of heterostructure was obtained by MOKE measurements either at spot A for TCFC/LSMO heterostructure, or at spot B for the LSMO film (see Fig. 1). The saturation field for TCFC/LSMO, $H_S \approx$ 1000 Oe, was typically much higher than for the LSMO film, $H_S \approx$ 20 Oe. The saturation magnetization of the TCFC/LSMO heterostructure is also much higher than the M_S of LSMO film (see also Fig. 1a; Ref. 12). Note, the influence of the underlying LSMO film at the spot A is screened for MOKE measurements by the TCFC film. When probing the LSMO film only (spot B Fig. 1), a change of magnetization sign was observed that points to an antiferromagnetic (antiparallel) magnetic ordering of layer magnetizations at the TCFC/LSMO interface of the heterostructure (Fig. 2).

Figure 3 shows hysteresis loops measured at the H-field directed along the easy axis. With a large sweeping range of external magnetic field (± 1.8 kOe), the hysteresis loop is approximately

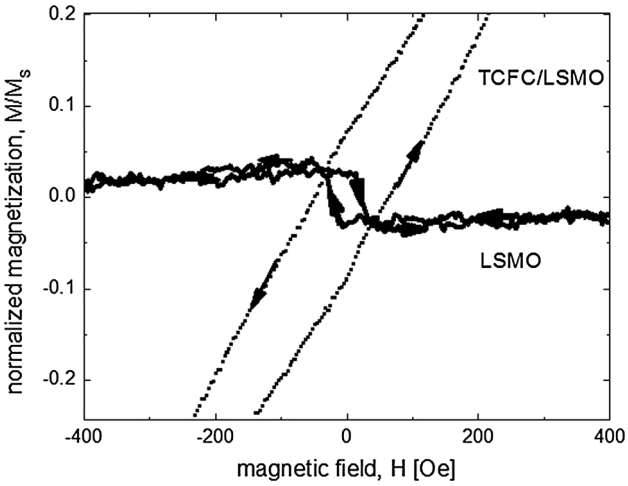

Fig. 2. Central part of the magnetization curves for both TCFC/LSMO (dotted line) and LSMO film (solid line) with ± 1.8k Oe sweeping range. Spot position A corresponds to the MOKE signal from the TCFC/LSMO heterostructure and (B) is spot position for LSMO film only (see Fig. 1). The external magnetic field is directed along the hard magnetization axis (ha). The arrows indicate the direction of the magnetic field change.

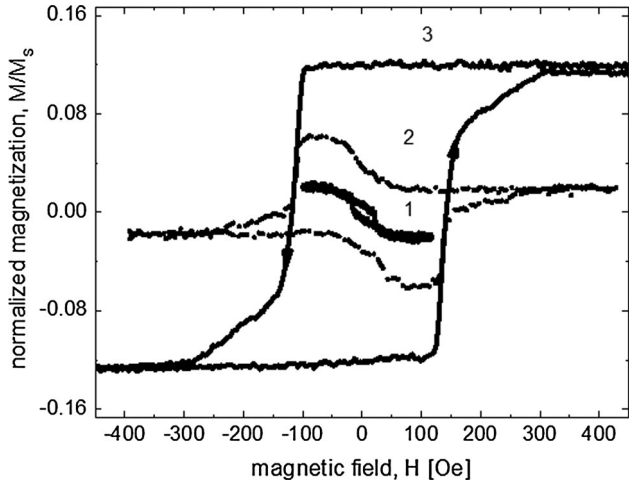

Fig. 3. Central part of the magnetization curve for the LSMO film (spot position B) for various sweep ranges: (1) ± 100 Oe, (2) ± 400 Oe and (3) ± 1.8 kOe. The external magnetic field is directed along the easy magnetization axis (ea). The arrows indicate the direction of the magnetic field sweep.

equal to the loop of the LSMO film without the TCFC superlattice on top. The width of the magnetization loops for both the TCFC/LSMO heterostructure and the LSMO film correspond to a coercive force of about 200 Oe due to influence of TCFC magnetization on LSMO film. The reason is possible influence of the stray field of the TCFC superlattice on magnetization of LSMO film. Quite a similar effect was observed for the TCFC/$Y_3Fe_5O_{12}$ heterostructure.[17] However, the mechanism of the interaction between layers is not clear yet. From Fig. 3, it is seen that with a smaller sweeping range, less than 400 Oe, the hysteresis loop of the TCFC/LSMO heterostructure exhibits a $M(H)$ dependence with an inverted sign as in the case when the magnetic field was directed along the hard axis (see Fig. 2). It indicates the antiferromagnetic nature of interaction between the layers. When the H-field sweeping amplitude was larger than 400 Oe, the magnetization curve for LSMO film repeated the shape of the magnetization loop of the TCFC superlattice (see Fig. 1b; Ref. 12).

Magnetometric Measurements

Figure 4a displays the magnetization loop measured by the VSM for a LSMO film deposited on NGO substrate. Magnetization loops are given for two orthogonal orientations of the magnetic field. The saturation magnetic field and magnetization are equal to H_S = 20 Oe, M_0 = 198 emu/cm^3, correspondingly. The coercive force is smaller than the saturation magnetic field due to the influence of the domain structure.

The VSM-measured magnetization curves of the LSMO/TCFC heterostructure for two opposite directions of magnetic field variation are shown in Fig. 4b. For magnetic field direction along the easy axis, the magnetization loop exhibits two steps corresponding to the reversal of magnetization in the soft (LSMO) and the hard (TCFC) magnetic layers. A similar behavior of magnetization was obtained in Ref. 18 by computer simulations performed for bilayer magnetic structures taking into account the coupling between the layers. The magnetization reversal process was investigated as a function of the strength of the interlayer exchange field and the ratio of the anisotropy constants of the magnetic layers. From the magnetic curve (Fig. 4b) it becomes obvious that a stable antiferromagnetic layer interaction takes place at a certain range of the external magnetic field. Taking into account the magnetization distributions discussed in Ref. 18, we can conclude that the reversal process proceeds more uniformly in the hard magnetic layer than in the soft one. In the former case, the magnetization undergoes a discontinuous change while its distribution is relatively uniform before the switching. In contrast, the soft magnetic layer is switched non-uniformly. The non-uniformity expands gradually, moving from the edges of the layer towards its center.

Magnetoresistance

The magnetoresistance of the TCFC/LSMO heterostructure was measured at T = 77 K for two directions of the applied magnetic field. For measurements of magnetoresistance, the same heterostructure but a different experimental lay out for current bias and magnetic field orientation was used (see the central inset to Fig. 5a and b). The resistance was measured over the diagonal direction of the substrate which corresponds to the magnetic hard axis. The changing of magnetoresistance was

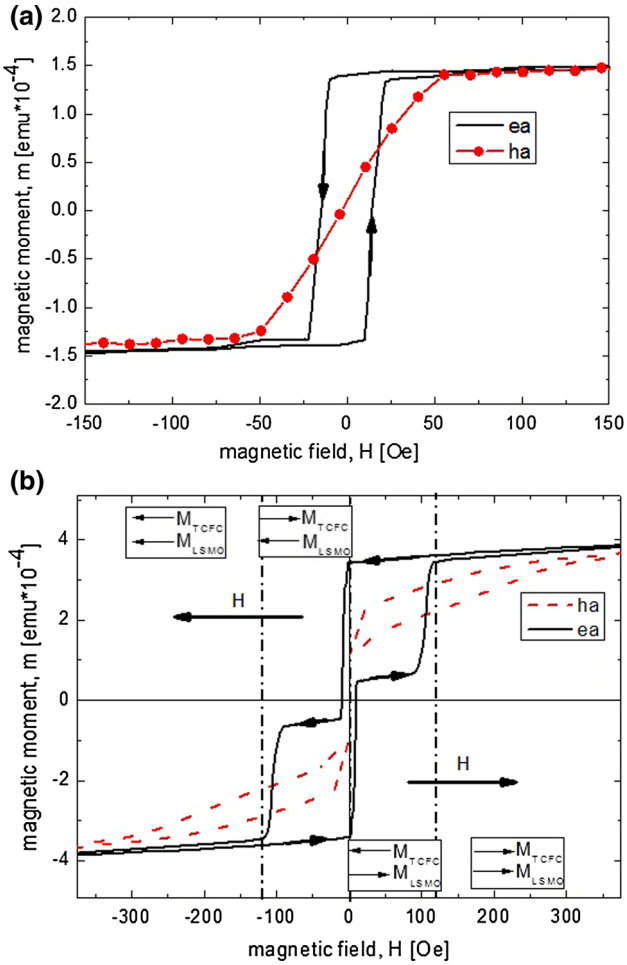

Fig. 4. The VSM magnetization curves for two structures: (a) LSMO film and (b) TCFC/LSMO heterostructure. The external magnetic field is directed either along either the hard axis or along the easy axis. The directions of the magnetization of the layers in heterostructure are shown in the inset of Fig. 4b.

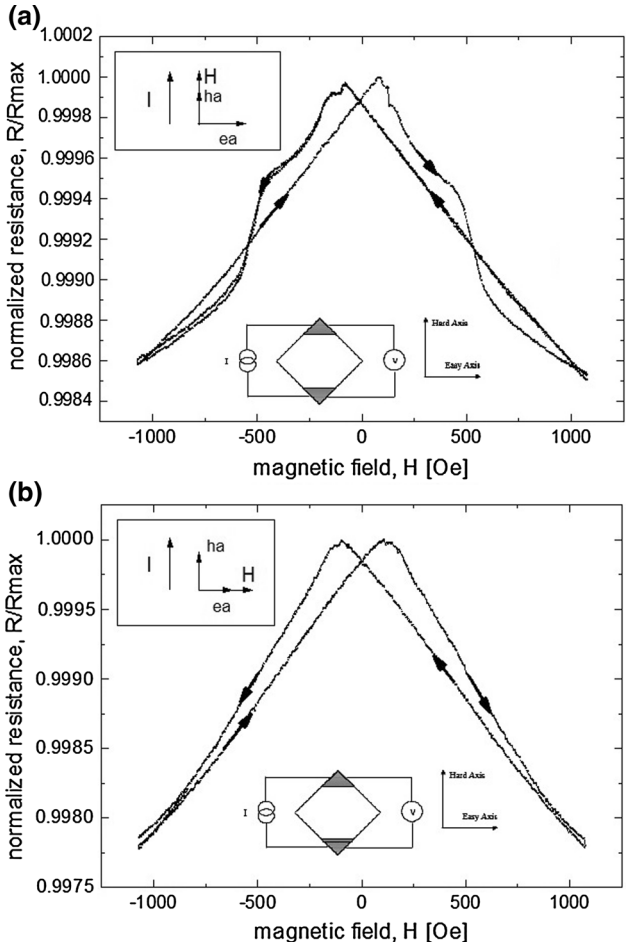

Fig. 5. Dependencies of the resistance on the magnetic field applied along either the hard (a) or easy (b) axes. The orientations of the magnetic field, dc biasing current directions as well the measurement scheme along with the topology of the structure are shown in the insets.

about 0.2% at $T = 77$ K which is smaller than at $T = 300$ K.

Let's first discuss the case in which the magnetic field is directed along the hard axis of magnetization (Fig. 5a). With a low field, there is a shift of the maximum of $R(H)$ which indicates the presence of ferromagnetism in the heterostructure. The distance between the peaks of $R(H)$ allows estimation of the coercive force of the heterostructure.[7] The slope of the $R(H)$ curves indicates the presence of colossal magnetoresistance in the manganite film.[13] The range of $R(H)$ change observed in the magnetic field (250–500 Oe) is probably caused by the switching the magnetization of the TCFC superlattice. In the second case (Fig. 5b), the magnetic field is directed along the easy axis. Again, there is an 80-Oe shift of the $R(H)$ maximum with respect to $H = 0$. But there is no change of $R(H)$ in the range of 250 to 500 Oe of the external magnetic field.

Figure 6 shows the difference of magnetoresistances for the magnetic field applied along the hard and the easy axes. The shape of the functions shown in Fig. 6 reflects the contribution of the interlayer interaction to magnetoresistance. Giant magnetoresistance (GMR) of the heterostructure and anisotropic magnetoresistance (AMR) are proportional to $(\cos\theta)^2$ where θ is the angle between magnetizations of the layers.[17–22] The change of the magnetoresistance caused by the switching of the TCFC film magnetization was observed for an applied magnetic field oriented along the hard axis (Fig. 5a). A similar behavior has been predicted in Ref. 8.

Ferromagnetic Resonance Studies

The FMR) spectrum for the heterostructure presented in Fig. 7 was measured at $\omega/2\pi = 9.74$ GHz and $T = 300$ K, with an in-plane dc magnetic field directed along the easy axis. It is seen in Fig. 7 that there are three regions of ferromagnetic ordering. The temperature dependencies of the resonance magnetic field H_0 for the three lines in the FMR spectra indicate that the low-field FMR line in Fig. 7 belongs to the TCFC superlattice. $H_0(T)$

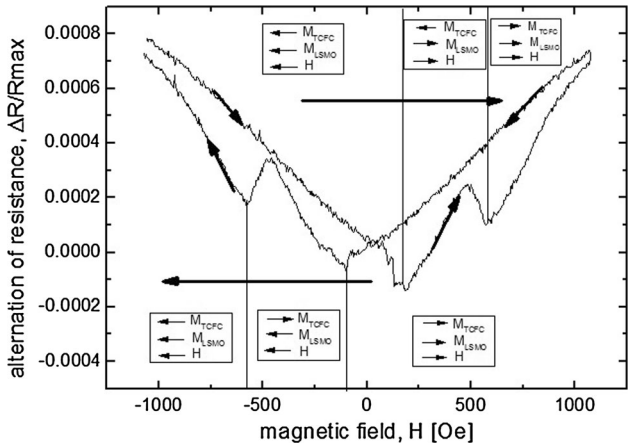

Fig. 6. Difference between magnetoresistance presented on Fig. 5a and b. The directions of magnetization in the heterostructure layers are shown in the insets.

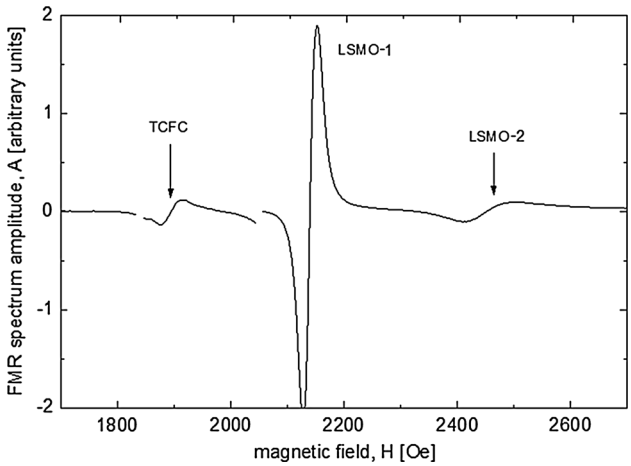

Fig. 7. FMR spectrum of the TCFC/LSMO heterostructure obtained under an external magnetic field directed along the easy magnetization axis, T = 300 K. The TCFC line is magnified ten times.

slowly decreases with reducing the temperature T and seems to indicates a high Curie temperature for the line (above room temperature). Two other lines belong to the LSMO film: LSMO-1 corresponds to the part located under the TCFC film, whereas LSMO-2 is related to the part of LSMO uncovered by TCFC. The numbers of spins associated with the spin-subsystems belonging to LSMO-1 and LSMO-2 are comparable. The estimation was carried out by calculation of the areas of corresponding FMR absorption spectral lines.

The FMR linewidths (ΔH) for LSMO-1 and LSMO-2 differ by 40–50 Oe. Since both LSMO-1 and LSMO-2 films are prepared on the same substrate and have the identical crystal quality, the observed difference in ΔH is related mostly to the interaction between TCFC and LSMO. A similar broadening of the FMR line for such a system with a ferromagnetic–normal metal interface was observed

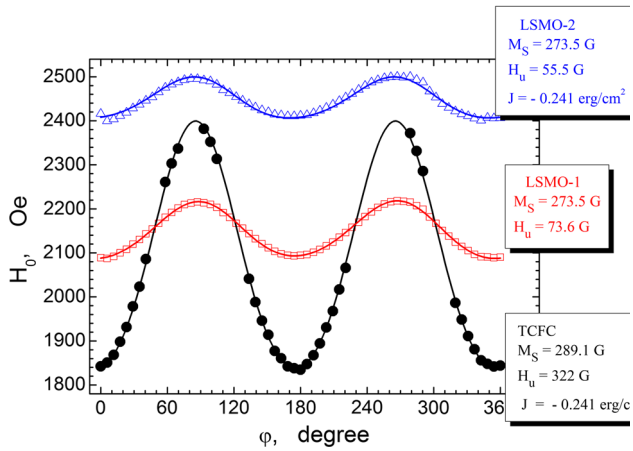

Fig. 8. Angular dependence of the resonance fields H_0 for the three FMR lines of the TCFC/LSMO heterostructure. The open triangles and squares correspond to LSMO-2 and LSMO-1 subsystems, respectively. Circles are the data for the TCFC superlattice. Solid lines show the calculated dependencies based on Eq. (1). Fitting parameters for magnetization M_S, uniaxial anisotropy field H_u and coupling energy J are shown in the insets.

earlier and theoretically explained in Ref. 23 by a spin current from the ferromagnetic to the normal metal generated by FMR.

Figure 8 shows the angular dependence of the resonance fields $H_0(\varphi)$ for all three spin subsystems. Within the magnetic field range of the FMR measurements (Fig. 7), all the spin subsystems in the structure are saturated and all magnetic moments are directed along the external magnetic field. The resonance ratio (1) derived in Ref. 24 can be used for estimation of the magnetic parameters of the films:

$$\left(\frac{\omega}{\gamma}\right)^2 = (H_0 + H_u \cos 2\varphi_u + H_c \cos 4\varphi_c) \times \left(4\pi M_0 + H_0 + H_u \cos^2 \varphi_u + H_c \frac{1+\cos^2 2\varphi_c}{2}\right) \quad (1)$$

where γ is the gyromagnetic ratio, $H_u = 2K_u/M_0$ and $H_c = 2K_c/M_0$ are the fields of the uniaxial planar and biaxial cubic anisotropy, respectively, with constants K_u and K_c, φ_u and φ_c corresponding to the angles between the uniaxial and biaxial anisotropy easy axes and the external magnetic field, respectively.

The minimum value of H_0 corresponds to magnetic field orientation along the easy axes. As seen in Fig. 8, the easy axes in all three spin subsystems are almost parallel with a deviation less than 2°–3°. The evolution of spin subsystems with the lower resonance fields describes the behavior of the FMR line corresponding to the LSMO-1, since the parameters of this line (the width and the resonance field) are characteristic for whole LSMO film on NGO substrate. Obtained magnetic parameters are shown in insets of Fig. 8.

In order to properly describe the FMR response for LSMO-2, the exchange interaction between LSMO and TCFC has been taken into account. For that, we considered the free energy including the joint action of Zeeman energy, magnetic anisotropy with the corresponding constants, and the component of bilinear exchange interaction with constant J. Uniform magnetizations of the films are also assumed.[24,25] The solution of the Landau–Lifshitz–Gilbert equation yields two resonance relations describing the FMR in the TCFC and LSMO-2 layers. These relations are analogous to Eq. (1) where H_0 should be replaced by the sums of the two terms $H_{01} + H_{J1}$ and $H_{02} + H_{J2}$ for the LSMO-2 and TCFC layers, respectively. Here, $H_{J1} = J/(M_1 d_1)$ and $H_{J2} = J/(M_2 d_2)$ are the effective interlayer exchange fields for the LSMO-2 and TCFC, correspondingly, and d_1 and d_2 are the thicknesses of these layers. The angular dependencies obtained from the resonance relationships for the LSMO-2 and TCFC layers which give the best fit to experimental data are shown in Fig. 8.

First, we calculated the FMR response of a single LSMO film (the LSMO-1 part). Then, using the obtained magnetization of LSMO layer along with the resonance relation that corresponds to the condition of interlayers exchange interaction, we calculated the angular dependence of the resonance fields for the LSMO-2 film. This procedure allowed determination of the exchange constant J. Finally, using the obtained J value, the angular dependence for the TCFC film is calculated and the M_2 value is deduced. As a result, the obtained data allow us to conclude that our structures with the TCFC/LSMO interface could be characterized by the antiferromagnetic interlayer exchange interaction with the negative constant $J = -0.24$ erg/cm.

CONCLUSION

Experimental data obtained on hybrid magnetic heterostructures made of epitaxial manganite $La_{0.7}Sr_{0.3}MnO_3$ thin film and intermetallic superlattice $(TeCo_2/FeCo)_n$ by means of the magneto-optical Kerr effect, magnetoresistance and ferromagnetic resonance show that the step-like peculiarities observed in magnetotransport characteristics are caused by the process of magnetization reversal at the interface between the manganite thin film and an intermetallic superlattice. The experimental data indicate the presence of an antiferromagnetic (antiparallel) magnetic state at the TCFC/LSMO interface. The energy of antiferromagnetic interlayer exchange interaction $J = -0.24$ erg/cm was estimated from FMR measurements. The influence of the stray field of the TCFC superlattice on magnetization of LSMO was observed. However, the mechanism of the interaction between layers is not clear yet.

ACKNOWLEDGEMENTS

The authors wish to thank A.M. Petrzhik, A.V. Shadrin, Y.V. Kislinskii and T.A. Shaihulov for help with experiment and useful discussion. Support by the Russian Foundation for Basic Research 16-29-14022, 17-02-00145 and Scientific School NSh-8168.2016.2 is acknowledged. Samples were partly processed with the support of the RENATECH technological network.

REFERENCES

1. J. Sinova and I. Žutić, *Nat. Mater.* 11, 368–371 (2012).
2. D.S. Jeong, R. Thomas, R.S. Katiyar, J.F. Scott, H. Kohlstedt, A. Petraru, and C.S. Hwang, *Rep. Prog. Phys.* 75, 076502 (2012).
3. D.E. Nikonov and I.A. Young, *J. Mater. Res.* 29, 2109 (2014).
4. B. Cui, Ch Song, G.A. Gehring, F. Li, G. Wang, C. Chen, J. Peng, H. Mao, F. Zeng, and F. Pan, *Adv. Funct. Mat.* 25, 864 (2015).
5. H.J. Mao, P.X. Miao, J.Z. Cong, C. Song, B. Cui, J.J. Peng, F. Li, G.Y. Wang, Y.G. Zhao, Y. Sun, L.R. Xiao, and F. Pan, *J. Appl. Phys.* 116, 053703 (2014).
6. Y. Dusch, N. Tiercelin, A. Klimov, S. Giordano, V. Preobrazhensky, and P. Pernod, *J. Appl. Phys.* 113, 17C719 (2013).
7. N. Tiercelin, Y. Dusch, S. Giordano, A. Klimov, V. Preobrazhensky, and P. Pernod, Strain-mediated magnetoelectric memory.*Nanomagnetic and Spintronic Devices for Energy Efficient Computing*, ed. S. Bandyopadhyay and J. Atulasimha (Hoboken: Wiley, 2016), p. 221.
8. A. Klimov, N. Tiercelin, V. Preobrazhensky, and P.H. Pernod, *IEEE Trans. Magn.* 42, 3090 (2006).
9. H. Le Gall, J. Ben Youssef, F. Socha, N. Tiercelin, V. Preobrazhensky, and P. Pernod, *J. Appl. Phys.* 87, 5783 (2000).
10. E. Quandt, A. Ludwig, D.G. Lord, and C.A. Faunce, *J. Appl. Phys.* 83, 7267 (1998).
11. N. Tiercelin, V. Preobrazhensky, P. Pernod, H. Le Gall, and J. Ben, Youssef. *J. Magn. Magn. Mater.* 210, 302 (2000).
12. I.V. Borisenko, V.V. Demidov, A.A. Klimov, G.A. Ovsyannikov, K.I. Konstantinyan, S.A. Nikitov, V.L. Preobrazhenskii, N. Tiercelin, and P. Pernod, *Tech. Phys. Lett.* 42, 113 (2016).
13. N. Tiercelin, V. Preobrazhensky, P. Pernod, and A. Ostachenko, *Appl. Phys. Lett.* 92, 062904 (2008).
14. Y. Dusch, V. Rudenko, N. Tiercelin, S. Giordano, V. Preobrazhensky, and P. Pernod, *Nanomater. Nanostruct.* 2, 44 (2012).
15. A.-M. Haghiri-Cosnet and J.P. Renard, *J. Phys. D Appl. Phys.* 36, R127 (2003).
16. I.V. Borisenko, M.A. Karpov, and G.A. Ovsyannikov, *Tech. Phys. Lett.* 39, 1027 (2013).
17. A.M. Churbanov, A.A. Klimov, A.V. Sadovnikov, E.N. Beginin, S.A. Nikitov, V.L. Preobrazhenskii, N. Tiercelin, and P. Pernod, *J. Commun. Technol. Electron.* 60, 999 (2015).
18. K.A. Zvezdin, *J. Phys. Solid State* 1, 120 (2000).
19. O. Jaoul, I.A. Campbell, and A. Fert, *J. Magn. Magn. Mater.* 5, 23 (1977).
20. A.P. Malozemoff, *Phys. Rev. B* 32, 6080 (1985).
21. R.E. Camley and J. Barnas, *Phys. Rev. Lett.* 63, 664 (1989).
22. J. Xiao, J. Jiang, and C.L. Ciien, *Phys. Rev. Lett.* 68, 3749 (1992).
23. Y. Tserkovnyak and A. Brataas, *Phys. Rev. Lett.* 88, 117601 (2002).
24. V.V. Demidov, G.A. Ovsyannikov, A.M. Petrzhik, I.V. Borisenko, A.V. Shadrin, and R. Gunnarsson, *J. Appl. Phys.* 113, 163909 (2013).
25. A.B. Drovosekov, O.V. Zhotikova, N.M. Kreines, D.I. Kholin, V.F. Meshcheryakov, M.A. Milyav, L.N. Romasheve, and V.V. Ustinov, *J. Exp. Theor. Phys.* 89, 986 (1999).